Inverse Source in a Multipath Environment

A. Cuccaro, R. Solimene, and R. Pierri
Dipartimento di Ingegneria Industriale e dell' Informazione
Seconda Unviersita' degli Studi di Napoli, via Roma 29, Aversa 81031, Italy

Abstract— Inverse source problem is addressed in a multipath environment. In particular, within a 2D scalar framework, the simple case multipath is due to a single thin PEC (Perfect Electric Conductor) cylinder scatterer deployed between the scene under investigation and the measurement line is considered. The role of the passive scatterer's position on the achievable performance is analysed for two different inversion schemes: back-projection and TSVD.

1. INTRODUCTION

As is well known, retrieving a current source from its radiated field is an ill-posed inverse problem [1]. It often happens that apart from the field due to the source, the fields produced by further scattering objects (generally unwanted) are collected as well. This can degrade the achievable performance as spurious artefact can crow the reconstructions. Nevertheless, if the in-homogeneous background is someway characterized (i.e., because it is artificially created) these waves can be exploited positively [2, 3].

In this contribution, we analyse the role played by a single PEC passive scatterers on imaging. Two inversion methods are considered. The first one consists in inverting the radiating operator which rigorously describes the radiation of unknown source in presence of a passive scatterer by a *TSVD* scheme. In the second one, the inversion is achieved by *BACK-PROJECTION*, which is one of the methods most commonly used in imaging. We will show how the achievable performance changes with the passive element compared to the free-space case, and how the the positions of the extra-scatterer acts.

2. MATHEMATICAL MODEL

The scenario of interest is depicted in Fig. 1. It consists of a scalar 2D geometry (invariant along the z-axis) including a infinitely long PEC cylinders (passive element) placed between the spatial region under investigation and the measurement line Γ_0. Accordingly, the radiated field (TM^y polarization is considered) can be expressed as

$$E(\underline{y}, k) = \int_{D_I} G_{BG}(\underline{y}, \underline{z}, \underline{p}, k) J(\underline{p}, k) d\underline{p} \tag{1}$$

where $E(\underline{y}, k)$ and $J(\underline{p}, k) = I(k) f(\underline{p})$ are the radiated field and the current distribution, respectively, k being the wavenumber. Note that, source frequency behaviour $I(k)$ is a priori known (for simplicity $I(k)$=1). D_I is the spatial domain where the source is assumed to reside, $\underline{y}$ is the observation point and $\underline{z}$ is the position of the passive element. The frequency ranges within [1, 1.5] GHz.

In order to exploit the effect due to grid, the passive element must be incorporated in the background model. In this case, the background is the whole environment depicted in Fig. 1 apart from the source. Therefore, if we assume that the PEC cylinder is "thin" in terms of wavelength (i.e., radius $\ll \lambda_{\min}$), the corresponding Green's function G_{BG} can be written as

$$G_{BG}(\underline{y}, \underline{z}, \underline{p}, k) = \frac{e^{-jk|\underline{y}-\underline{p}|}}{\sqrt{|\underline{y}-\underline{p}|}} + a_0(k) \frac{e^{-jk|\underline{y}-\underline{z}|} e^{-jk|\underline{z}-\underline{p}|}}{\sqrt{|\underline{y}-\underline{z}|}\sqrt{|\underline{z}-\underline{p}|}} \tag{2}$$

with $a_0(\cdot)$ the first term of the cylindrical harmonic expansion of scattering from the passive element.

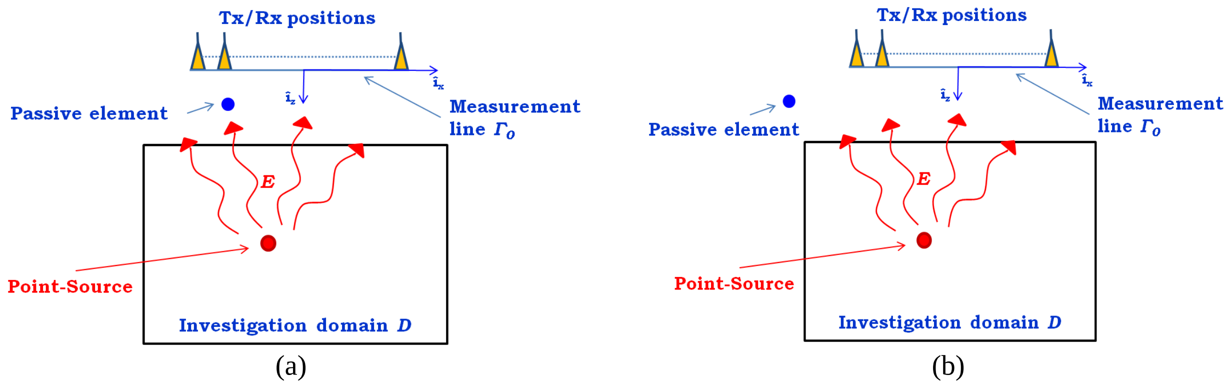

Figure 1: Geometry of the problem. (a) Passive element in $(-1\lambda_{\max}, -5\lambda_{\max})$. (b) Passive element in $(-12\lambda_{\max}, -5\lambda_{\max})$. Investigation domain $D_I = [-8\lambda_{\max}, 8\lambda_{\max}] \times [-10\lambda_{\max}, -26\lambda_{\max}]$. Measurement line $\Gamma_0 = [-4\lambda_{\max}, 4\lambda_{\max}]$ is located at stand-off distance of $10\lambda_{\max}$ from the investigation domain. Source in $(2\lambda_{\max}, -15\lambda_{\max})$.

3. BACK-PROJECTION

By performing the inversion scheme with back-projection the reconstruction can be written as

$$I(\underline{p}) = \int_{\Omega_k} \int_{\Gamma_0} E(\underline{y}, k) \left(G_{BG}(\underline{y}, \underline{z}, \underline{p}, k)\right)^* d\underline{y} dk \tag{3}$$

This image is the sum of four contributions that we address as I_{11}, I_{12}, I_{21} and I_{22}. Below, we analyze the kernels (point spread functions) of the various terms.

3.1. Term 11

$$I_{11}(\underline{p}) = \int_{\Omega_k} \int_{\Gamma_0} \frac{e^{jk\left(-|\underline{y}-\underline{x}|+|\underline{y}-\underline{p}|\right)}}{\sqrt{|\underline{y}-\underline{x}||\underline{y}-\underline{p}|}} d\underline{y} dk \tag{4}$$

Henceforth, the phase term of each contribution of the image will be indicated briefly as $\Phi(k, \underline{y})$. It can be shown that Eq. (4) provide a significant contribution in the reconstruction when $\nabla_{k,\underline{y}}(\Phi) = 0$. This condition explicitly becomes

$$\frac{\partial \Phi(k, \underline{y})}{\partial k} = 0 \Longrightarrow |\underline{y} - \underline{x}| = |\underline{y} - \underline{p}| \tag{5}$$

$$\frac{\partial \Phi(k, \underline{y})}{\partial \underline{y}} \cdot \hat{i}_x = 0 \Longrightarrow \widehat{y - x} \cdot \hat{i}_x = \widehat{y - p} \cdot \hat{i}_x \tag{6}$$

The aim is to find the conditions that satisfy the equations just written. In other words, fixed the measurement set-up (passive element $\underline{z}$, investigation domain D_I and extent of the measurement line Γ_0), we check whether a stationary-point exists or not. The first and the second equation are constraints on the distance (henceforth denoted as "modulus condition" $c.m$) and on the position (henceforth denoted as "position condition" $c.p$), respectively. Analyzing these conditions we can assert that for each observation $\underline{y}$ and wave-number k, the max value produced from integral I_{11} is located in a neighbourhood of the source point $\underline{x}$. Therefore, there is focusing on the source as shown clearly in Fig. 2(a).

3.2. Term 12

$$I_{12}(\underline{p}) = \int_{\Omega_k} \int_{\Gamma_0} a_0^*(k) \frac{e^{jk\left(-|\underline{y}-\underline{x}|+|\underline{y}-\underline{z}|+|\underline{z}-\underline{p}|\right)}}{\sqrt{|\underline{y}-\underline{x}||\underline{y}-\underline{z}||\underline{z}-\underline{p}|}} d\underline{y} dk \tag{7}$$

Reconstruction (7) becomes significant when

$$\frac{\partial \Phi(k, \underline{y})}{\partial k} = 0 \Longrightarrow -|\underline{y} - \underline{x}| + |\underline{y} - \underline{z}| + |\underline{z} - \underline{p}| = 0 \tag{8}$$

$$\frac{\partial \Phi(k, \underline{y})}{\partial \underline{y}} \cdot \hat{i}_x = 0 \Longrightarrow \widehat{y - x} \cdot \hat{i}_x = \widehat{y - z} \cdot \hat{i}_x \tag{9}$$

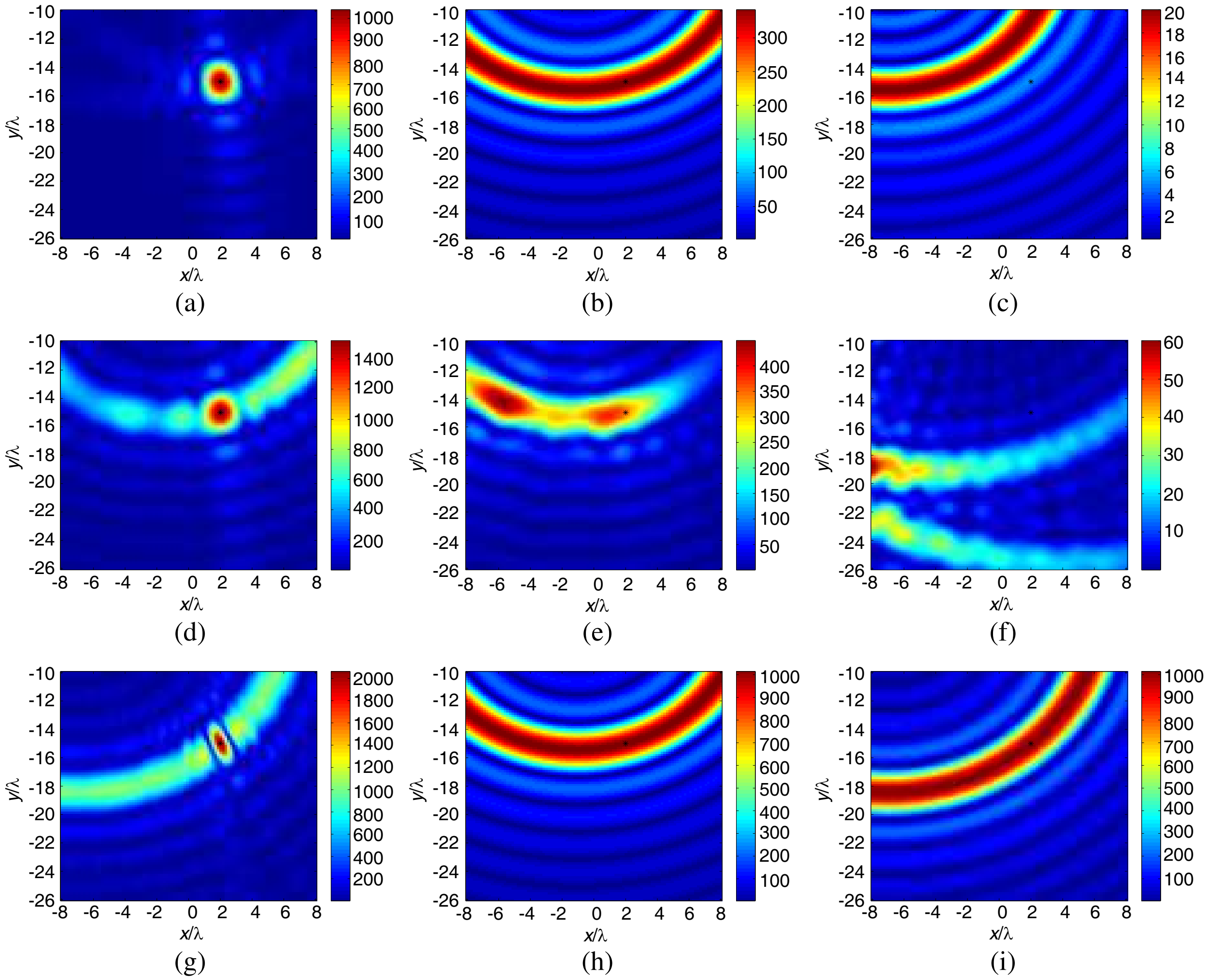

Figure 2: Reconstruction for scene layout depicted in Fig. 1(a): (a) I_{11}. (b) I_{12}. (e) I_{21}. (h) I_{22}. (d) $(I_{11} + I_{12} + I_{21} + I_{22})$. Reconstruction for scene layout depicted in Fig. 1(b): (a) I_{11}. (c) I_{12}. (f) I_{21}. (i) I_{22}. (g) $(I_{11} + I_{12} + I_{21} + I_{22})$. In all the figures actual source's position is displayed as black asterisk.

When the passive element is placed in front the measurement line, the above equations say there will be a dominant artefact in the reconstruction characterised from a circular geometry. Moreover, it includes the source position (see Fig. 2(b)). Although the artefact is due to a stationary-point, we observe that here this situation happens only for few observation points. This explains why the amplitude dynamic of I_{12} depicted in Fig. 2(b) is lower than the one showed in Fig. 2(a). If the inhomogeneity is placed outside the measurement line, from $c.m$ and $c.p$ conditions, we expect again a circular artefact in the image I_{12}. However unlike the case already examined, here the source position does non belong to the it (see Fig. 2(c)). Finally, we observe that this specific artefact has a dynamic influenced from the position of passive element, and its location within investigation domain depends from the relative position between passive element $\underline{z}$ and the source $\underline{x}$.

3.3. Term 21

$$I_{21}(\underline{p}) = \int_{\Omega_k} \int_{\Gamma_0} a_0(k) \frac{e^{jk\left(-|\underline{y}-\underline{z}|-|\underline{z}-\underline{x}|+|\underline{y}-\underline{p}|\right)}}{\sqrt{|\underline{y}-\underline{z}||\underline{z}-\underline{x}||\underline{y}-\underline{p}|}} d\underline{y} dk \tag{10}$$

The image (10) assumes the maximum value when

$$\frac{\partial \Phi(k, \underline{y})}{\partial k} = 0 \Longrightarrow -|\underline{y}-\underline{z}| - |\underline{z}-\underline{x}| + |\underline{y}-\underline{p}| = 0 \tag{11}$$

$$\frac{\partial \Phi(k, \underline{y})}{\partial \underline{y}} \cdot \hat{i}_x = 0 \Longrightarrow \widehat{y-z} \cdot \hat{i}_x = \widehat{y-p} \cdot \hat{i}_x \tag{12}$$

Once again $c.m$ and $c.p$ conditions are examined in two different scenarios. For the geometry depicted in Fig. 1(a), we can assert that each observation points is stationary hence more artefacts appear in the image I_{21}, including the one focuses on the source point $\underline{x}$ (see Fig. 2(e)). Instead, for the scenario shown in Fig. 1(b) no stationary-point is allowed. Therefore, as depicted in Fig. 2(f), we deduce a lower dynamic reconstruction. Moreover, although it would not seem, the nature of artifact is again circular.

3.4. Term 22

$$I_{22}(\underline{p}) = \int_{\Omega_k} \int_{\Gamma_0} |a_0|^2 \frac{e^{jk\left(-|\underline{z}-\underline{x}|+|\underline{z}-\underline{p}|\right)}}{\sqrt{|\underline{z}-\underline{x}||\underline{z}-\underline{p}|}} d\underline{y} dk \tag{13}$$

In this specific case, Eq. (13) provide a relevant contribution if

$$\frac{\partial \Phi(k, \underline{y})}{\partial k} = 0 \Longrightarrow |\underline{z}-\underline{x}| = |\underline{z}-\underline{p}| \tag{14}$$

while the condition $c.p$ not provide any additional information. The latter equation implies an artefact of circular geometry (see Fig. 2(h)) similar to the reconstruction of the term I_{12}. However, its dynamic is very different because in Fig. 2(b) the artefact is due to a limited number of receiver positions $\underline{y}$, whereas here it is the same for all the elements of the measurement line Γ_0. Finally, we observe that the nature of the artefact is not depend from the passive element $\underline{z}$ (Figs. 2(h)–(i)).

Eventually, we can foresee that many artefacts can corrupt the reconstructions, as show in Figs. 2(d)–(g). Nevertheless, a resolution improvement occurs when the extra point scatterer is positioned as in scenario Fig. 1(b).

4. TSVD STRATEGY

Since the Eq. (1) is a linear integral operator, another possible inversion scheme is the TSVD. With this approach, the reconstruction can be expressed as

$$I(\underline{p}) = \sum_{n=0}^{N_T} \frac{\langle E, v_n \rangle}{\sigma_n} u_n \tag{15}$$

where $I(\underline{p})$ represents the regularised reconstruction of $J(\cdot)$, $(v_n, u_n)_{n=0}^{\infty}$ form ortho-normal bases in the data and unknown space, respectively, and $(\sigma_n)_{n=0}^{\infty}$ is the set of singular value. N_T is a truncation index determining the degree of regularization of the solution.

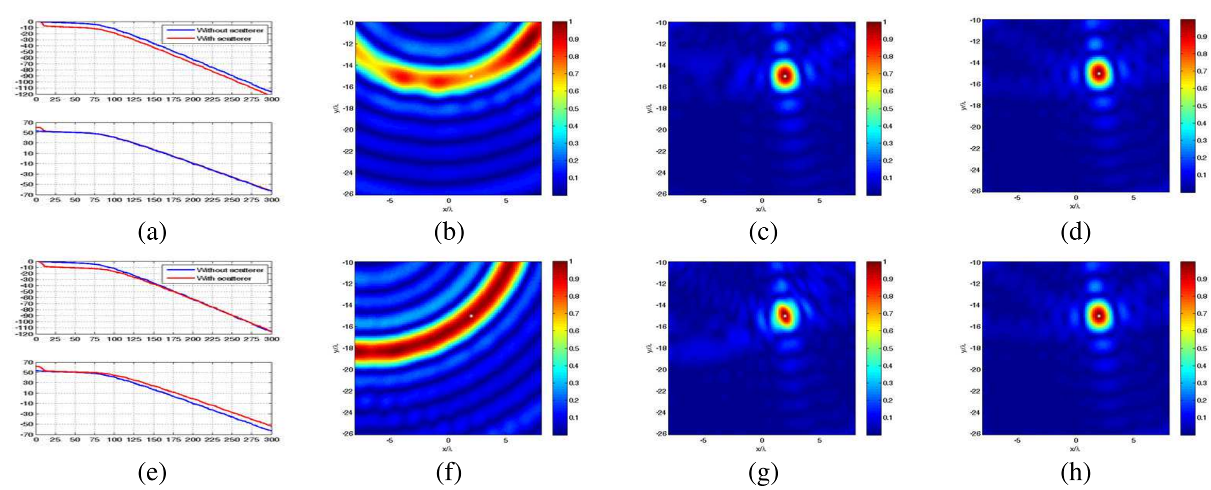

Figure 3: (Top panel) The geometry is the same of Fig. 1(a). (a) Singular values behaviour. (b) Reconstruction with passive element choosing $\gamma = -5$ dB. (c)–(d) Reconstruction ($\gamma = 44$ dB) with and without passive element, respectively. (Bottom panel) The geometry is the same of Fig. 1(b). (e) Singular values behaviour. (f) Reconstruction with passive element choosing $\gamma = -5$ dB. (g)–(h) Reconstruction (choosing $\gamma = 44$ dB) with and without passive element, respectively. In all the figures actual source's position is displayed as white asterisk.

We begin our analysis from the scenario depicted in Fig. 1(a). The singular values behavior reported in Fig. 3(a) suggests that the scatterer is responsible of a steep climb in the first part of singular values (red line). To understand the effect of this phenomena on imaging, in Fig. 3(b) is depicted $I(\underline{p})$ choosing a suitable threshold γ in order to consider only the singular values corresponding to that rise. Comparing Fig. 2(h) with Fig. 3(b), we can say that the pedestal in the singular value behavior provides merely the equivalent artefact of the terms I_{22} achieved with back-projection strategy. Going beyond, that is adding about 10 more singular values, the two singular value curves are almost identical (Fig. 3(a) not normalized trend). Therefore, regardless of the choice of the threshold, the value and the number of singular values used for the reconstruction is the same. In order to compare actual performance in two different contexts, we choose the truncation threshold $\gamma = 44\,\mathrm{dB}$. Although the number of singular values is similar in both configurations (about 90), regardless of the presence or absence of the passive element, the two reconstructions are similar (Figs. 3(c)–(d)).

In the bottom panel of Fig. 3 are depicted the reconstruction when the passive element $\underline{z}$ is placed outside the measurement line. Observing the singular value behavior shown in Fig. 3(e), it can be recognised that the passive element is responsible once again of a climb, but also of a bulge. In other words, passed a critical threshold value, the curve of singular values with the passive element is always higher than the one without passive element (Fig. 3(e) (not normalized behavior). This suggests that choosing properly the truncation threshold, with the passive element the performance achievable can improve. In Fig. 3(f) is shown the reconstruction when the threshold $\gamma = -5\,\mathrm{dB}$ (normalized behavior). Since in this case, in the inversion scheme are considered only about 10 singular values, the reconstruction achieved again corresponds essentially to the I_{22} depicted in Fig. 2(i). Finally, in order to compare actual performance in two different contexts, we choose the truncation threshold $\gamma = 44\,\mathrm{dB}$. Although with passive element the number of singular values is just 15 more than that in free space, the image shown in Fig. 3(g) is slightly narrower than Fig. 3(h).

ACKNOWLEDGMENT

This work was supported in part by POR Campania FSE 2007/2013-Embedded System.

REFERENCES

1. Bertero, M., "Linear inverse and ill-posed problems," *Advances in Electronics and Electron Physics*, Vol. 75, 1120–1989, Ed., P. W. Hawkes, Academic, New York, 1989.
2. Gennarelli, G., R. Persico, and F. Soldovieri, "Effective imaging systems based on periodic lattices," *Applied Physics Letters*, Vol. 104, 2014.
3. Cheney, M. and R. J. Bonneau, "Imaging that exploits multipath scattering from point scatterers," *Inverse Problems*, Vol. 20, 1691–1711, 2004.